

ISLAND WAKES OBSERVED FROM HIGH-FREQUENCY CURRENT MAPPING RADAR

By Sophia T. Merrifield, Patrick L. Colin, Thomas Cook, Carlos Garcia-Moreno, Jennifer A. MacKinnon,
Mark Otero, Travis A. Schramek, Mika Siegelman, Harper L. Simmons, and Eric J. Terrill



Aerial photo looking north on Kayangel, a four-island atoll that sits 35 km north of Babeldaob, the largest island of the Republic of Palau. Accessible only by boat, weather permitting, it is home to the northernmost offgrid site of Palau's high-frequency radar observatory. The station faces east and sits 15 m away from the reef on one of Kayangel's uninhabited islets, where it provides unobstructed measurements of radial surface currents out to 160 km.

ABSTRACT. The interaction of large-scale oceanic flows with remote island chains can lead to turbulent wakes, enhanced vorticity production, and significant increases in biological productivity. This study showcases the range of flow conditions captured by surface current mapping high-frequency (HF) radar systems deployed around the main island group of Palau in the western Pacific. The radar array captures strong tidal and inertial flows, both near- and offshore, as well as the spatial and temporal variability associated with the synoptic geostrophic flow interacting with the island group. Surface currents measured by HF radar are significantly correlated to currents in the upper 100 m of the ocean water column, as observed with a concurrent mooring, such that the resulting surface spatial maps provide insight on the wake flows of the island across a significant portion of the upper ocean. Composite averages of eastward and westward incident flow show flow-splitting and reconnection 60 km upstream and downstream of the island group, respectively. Surface current variability observed by the radar array includes topographically blocked flow, flow separation and acceleration through passages in the island chain, eddy dipole structure, and coastal eddies with Rossby numbers of 5. The range of variability near the island chain is reflective of the complex incident flow, which encounters Palau from all directions and changes on timescales of hours to weeks. A high-resolution model qualitatively agrees with the HF radar observations and shows vorticity filaments generated downstream of the island passages.

IN PLAIN WORDS. Three high-frequency radar systems measuring surface currents capture a diverse set of flow features associated with the interaction of large-scale currents with the island nation of Palau in the western Pacific. Surface currents are significantly correlated to flows in the upper 100 m and bypass the island chain by splitting and reconnecting approximately 60 km up- and downstream, respectively. Narrow channels in the island chain produce strong wake signatures that are captured by high-resolution models; island wakes have important connections to biological productivity and ocean energetics.

INTRODUCTION

In the Western Pacific Ocean, a number of Micronesian Archipelago island groups are situated within the paths of the North Equatorial Current (NEC) and the North Equatorial Countercurrent (NECC). In this region, the NEC and NECC flows are predominately westward and eastward, respectively, and the former bifurcates into the Kuroshio and Mindanao boundary currents near the Philippine coast (Figure 1A). On the large scale, aspects of the NEC and the NECC are well studied, including vertical structure (e.g., Schönau and Rudnick, 2015; Zhang et al., 2017), seasonal (Hsin and Qiu, 2012) and inter-annual (Qiu and Lukas, 1996) variability, and the resulting biological impacts (Sugimoto et al., 2001). However, relatively little is known about the near-

field development and influence of oceanic wakes at these remote island chains. Analogue studies in other locations have documented diverse wake conditions (Pattiaratchi et al., 1987; Hsu et al., 2019) and a physically driven increase in biological productivity (e.g., Arístegui et al., 1997; Gove et al., 2016).

Oceanic flow-topography interactions are often studied in the framework of unstratified, uniform flow past a cylinder, where the development of a wake in the lee of an obstacle scales with the Reynolds number ($Re = UL/\nu$). Here, Re is defined in terms of the incident flow velocity, U , the characteristic horizontal length scale of the obstacle, L , and the horizontal eddy viscosity, ν . Using the horizontal eddy viscosity in the definition of Re reflects the turbulent nature of the incident oce-

anic flow. As Re increases, flows encountering an obstacle separate, vortices form and shed, and flows become increasingly turbulent and irregular (Kundu and Cohen, 2002). This idealized framework, however, proves insufficient to accurately describe flow near archipelagos for several reasons: incident oceanic flows are often broadband in frequency and wavenumber content, the fluid is stratified, and topographic features are complex.

The observations presented in this study were collected at Palau, an island group characterized by complex topography with both shallow reef environments and steep bathymetric gradients extending to 4–8 km depth (Figure 1B). There are passages in the island chain between the main atoll system and nearby neighboring islands and two channels in the north: Euchelet Ngeruangl (~800 m maximum depth), which separates Kayangel and Velasco Reef, and Kekelel Eichel (~300 m maximum depth), which separates Kayangel from the main island (Figure 1C). In the south, a channel (~400 m maximum depth) separates Angaur from the main island. This channel is known for strong flows often exceeding 2 m s^{-1} (Schramek, 2018; Figure 1D), and it includes Hydrographer's Bank, an isolated region within the channel that rises to approximately 25 m depth. The incident flows associated with the NEC and NECC both have a dominant two-layer depth structure, are strongly eddying via mesoscale meanders, and vary on timescales of hours to years (Schönau and Rudnick, 2015).

The nature of the resulting wake at Palau is complex, broadband, and scale dependent. The Rossby number used to characterize the wake here is defined as the ratio of relative vorticity to planetary vorticity, $Ro = |\zeta|/f$, where $\zeta = \partial_x v - \partial_y u$, f is the Coriolis frequency, and u and v are the zonal and meridional components of the current vector, respectively. Recent studies show that the flows rounding

the northern point of Velasco Reef generate small-scale (~1 km) wake eddies of both signs of relative vorticity and $Ro = 30$, and suggest the relative magnitude of tidal and low-frequency flows is important in the nature of the wake (MacKinnon et al., 2019). Johnston et al. (2019, in this issue) observed wake eddies of similar scale at Peleliu, near the southern point of Palau, and documented the cascade of energy through the submeso-scale to turbulence. Zeidan et al. (2019) used velocity profiles derived from buoyancy glider surveys along transects 40 km east and west of Velasco Reef to determine flow acceleration, lee return flows, and mean $Ro \sim 0.3$ in the wake. All three studies provide important perspectives on the temporal and spatial scales of the wake and vorticity production at Palau; however, the connection between small-scale tidal eddies generated at topography and the downstream, larger-scale wake of the island chain remains uncharacterized. The time-space HF radar observations presented here provide new insights into the surface structure of the wake and context for the incident flows that interact with Palau.

Observations presented in this study were collected as part of the Office of Naval Research (ONR)-funded Flow Encountering Abrupt Topography (FLEAT) Departmental Research Initiative, which addresses the cascade of energy from large-scale ocean currents to smaller-scale motions as these flows interact with topography at island groups. In this article, we first describe the HF radar systems and data processing to obtain total surface current vectors, then discuss flow variability and vorticity generation in case studies to demonstrate the range of observed features. Finally, we describe the implications of the observations in the context of the energy cascade and an introduction to model downscaling efforts.

OBSERVATIONS

Three HF radar systems were installed at Kayangel (8.06°N, 134.71°E), Melekeok (7.49°N, 134.64°E), and Angaur (6.91°N, 134.15°E), on the northern, central, and southern regions of the island chain, respectively (Figure 1B). CODAR Ocean Sensor's long-range SeaSondes were installed at all sites. The systems operate

near 5 MHz, and the network is configured to produce hourly averaged sea surface current measurements with 6 km horizontal resolution and up to 160 km range offshore. Because the measurement depends on observation of the Doppler shift of the Bragg ocean wavelength, which reflects the radio signal, the operating frequency dictates the effective sampling depth (e.g., Crombie, 1955; Stewart and Joy, 1974; Barrick et al., 1977). For 5 MHz systems, this equates to the signal most influenced by currents in the upper 2.4 m and a weighted average depth of 1.3 m based upon accepted models of upper ocean shear (for a range of expected shear profiles, the observed Doppler shift is a weighted depth average between 8% and 16% of the ocean wave responsible for the Bragg return). Based on validation studies of HF radar-derived surface currents, we assume a noise level or uncertainty of $\pm 6 \text{ cm s}^{-1}$ in the total velocity solutions (Emery et al., 2004; Ohlmann et al., 2006).

The Multiple Signal Classification (MUSIC) direction finding algorithm (Schmidt, 1986) is applied to the measured backscatter data to resolve the

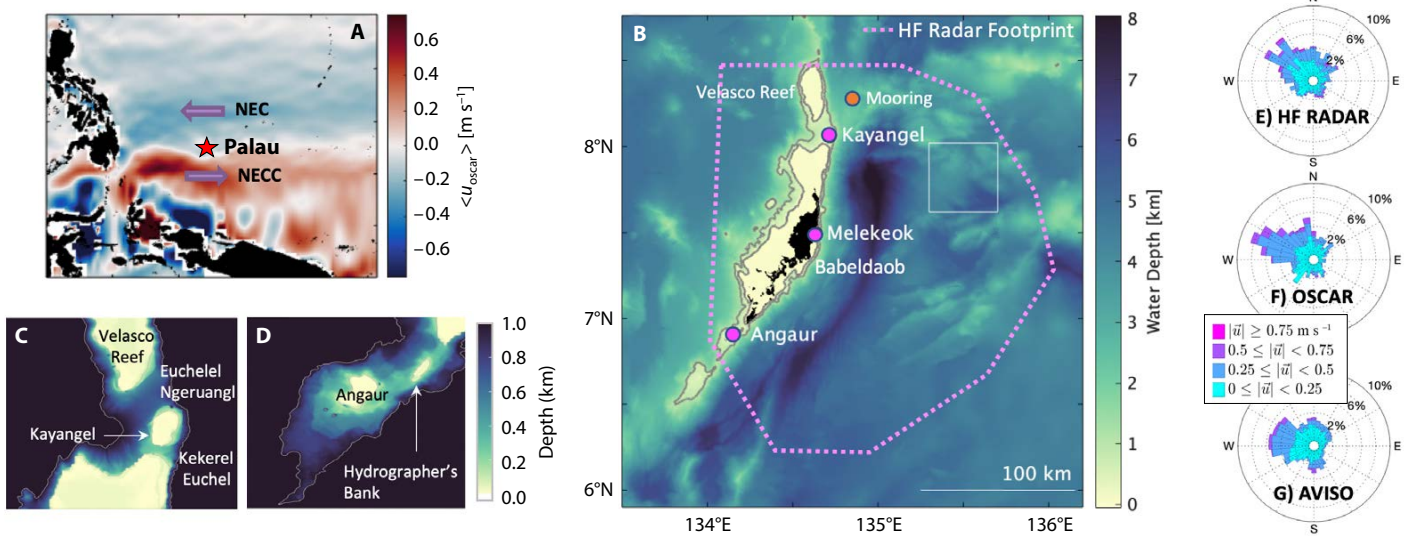


FIGURE 1. (A) Schematic of the North Equatorial Current (NEC) and the North Equatorial Countercurrent (NECC) relative to the location of Palau using averaged zonal Ocean Surface Current Analysis Real-time (OSCAR) currents (2016–2019). (B) Map of bathymetry at Palau. (C) Kekelel Euchel and Euchelee Ngeruangl channels. (D) Hydrographers Bank. Locations of the mooring and HF radar stations at Kayangel, Melekeok, and Angaur are shown as pink circles in (B). Bathymetry data have 100 m resolution and include multibeam from ship surveys and Smith and Sandwell (1997). Current velocity roses (direction current going toward) are shown for the white box in 1B for (E) HF radar observations with a 33-hour bin average applied to remove tides, (F) OSCAR, (G) Archiving, Validation and Interpretation of Satellite Oceanographic Data (AVISO) over the three-year record.

direction of the radial surface currents observed at each radar site. The hourly radial files are comprised of solutions that are filtered by a three-hour moving average to reduce noise. Each site's radial solutions are telemetered back to Scripps Institution of Oceanography (SIO) in near-real time and mapped onto an equidistant cylindrical grid with nominal resolution of 6 km using a least squares solution to create total velocities (Barrick and Lipa, 1983; Gurgel, 1994). The total solutions are typically available within two hours of real time (1.5 hours of which are due to the chosen three-hour moving average) and form the synoptic surface current maps that are used in subsequent analyses. Quality control is implemented at all stages of processing, including on site at each radar station (signal processing and calibration with measured patterns), upon ingestion at SIO (file integrity), and during total processing (velocity thresholding and solution stability; geometric dilution of precision [GDOP] < 1.25; see Chapman et al., 1997, for definition of GDOP as it pertains to HF radar).

The radar network was tested during the first quarter of 2016 and entered into scientific use in June of 2016. Although station locations were chosen to maximize the potential two-dimensional surface current coverage map, unique challenges of the austere nature of western Pacific islands resulted in inadvertent downtime. Poor radial coverage has plagued the system during some periods of the time series as a result of increased noise figures, presumably from mainland Asia to the west and a reflective ionosphere that is favorable for increased clutter. Long-range ground wave radars used for oceanographic sampling have recently been found to be influenced by ionospheric multipath reverberation from their own transmissions. This phenomena depends on current space weather conditions, with the reflective layers located at distances of O(60–300 km) above Earth's surface. Much of the downtime can be directly attributed to power

outages caused by extended periods of cloud cover during Palau's rainy season and shadowing of the photovoltaic panels by overgrowth. Although it was grid-connected, there were also prolonged power outages at Melekeok due to issues with the national power grid.

In addition to power outages, variability in range of radial coverage can also be detrimental to generating consistent cov-

erage in total solutions. A significant drop in the number of radial solutions being produced by a station inherently reduces the overlap area that enables total surface current calculations. An example of this is the diurnal reduction in range of radial velocities due to noise that overwhelmed the signal, potentially caused by ionospheric clutter. This behavior can be observed in many HF radars operating on similar frequency bands throughout Southeast Asia (Chung et al., 2017). Changing antenna radiation patterns and weak backscatter during low winds also played a role in reduced spatial and temporal coverage.

In order to remove some of the variability in coverage, grid points were filtered out if temporal coverage did not exceed at least 10% of the three-year sampling record. Because of the irregular sampling, our analysis is presented as case studies and composite averages during periods when data coverage and quality were relatively high. Further details about the HF radar installation and data processing are provided in the online supplementary materials.

FLOW VARIABILITY

The incident flows at Palau vary in strength and direction over the measurement record, with a predominance in flow toward the northwest (Figure 1E). Satellite-derived current products from Ocean Surface Current Analysis Real-time (OSCAR) and Archiving, Validation and Interpretation of Satellite Oceanographic Data (AVISO) sea surface heights

“ While the majority of coastal studies that use this technology are located in regions dominated by shelf physics...our study observes ocean surface currents in a region of steep boundary topography, with average water depths of 4 km. ”

show similar patterns in the incident currents (Figure 1F,G); directional differences are attributed to the large spatial averaging scales of the gridded products that don't capture the narrow bathymetry of Palau. The surface flows measured by HF radar near Palau are energetic and in strong agreement with moored observations of velocity averaged over the upper 16–36 m (Figure 2A,B). The surface currents exhibit prominent inertial and tidal variability, consistent with moored observations presented in Siegelman et al. (2019, in this issue). Rotary frequency spectra (Figure 2C) show three significant peaks in both the radar and mooring data: dominant semidiurnal and diurnal tidal constituents, and a peak at f_{in} , the local inertial period (~86 hours at 8°N). The inertial peak is polarized (dominant clockwise rotation) and broadband ($0.8 f_{in} - 1.2 f_{in}$), consistent with near-inertial variability and phase modification of the inertial frequency by meso-scale vorticity, $f_{eff} = f + \zeta$ (Weller, 1982). The strength of the tidal and inertial flows, estimated by bandpass filtering the total velocities, are on average, 10–15 cm s⁻¹.

The tides are mixed semidiurnal and diurnal, with dominant constituents M2 and K1, respectively. Harmonic fits applied to the three-year records capture very little variance of the tidal currents because most of the energy in these bands are not phase locked. The complex bathymetry at Palau makes it a region susceptible to internal tide generation.

An important finding about the deep-water study region is that the surface flows measured by HF radar capture the upper layer currents down to the seasonal thermocline, which is around 100 m depth (Figure 3A,B). There is very little shear or current rotation with depth, which suggests that wind-driven physics

play a minimal role in the surface current variability. The subtidal flow, estimated by applying a 33-hour running average to the mooring and HF radar currents, are significantly correlated in the upper 100 m, with a maximum correlation coefficient of 0.67 and 0.84 for the zonal and meridional components, respectively (Figure 3C). The mooring location is approximately 12 km east of the shallow sunken atoll Velasco Reef (Figure 1B), which asymmetrically influences the depth structure of strongly zonal relative to meridional flows and accounts for the discrepancy in correlation coefficients.

Strong spatial variability within the HF footprint captured over the three-year

data set is attributed to a range of flow conditions that result from island-flow interaction. Here, we focus on characterizing a subset of these events. Specifically, we present descriptions of the flow during blocked (westward-incident flow; Figures 4A and 5A,B) and wake (eastward-incident flow; Figures 4B, 5C,D, and 6A) conditions, and eddying features with strong vorticity signatures (Figure 5). AVISO geostrophic currents (daily temporal, 1/4° spatial resolution) are used for large-scale context of the incident flow and to demonstrate the ageostrophic nature of the surface flow near the island.

Predominant incident flows toward

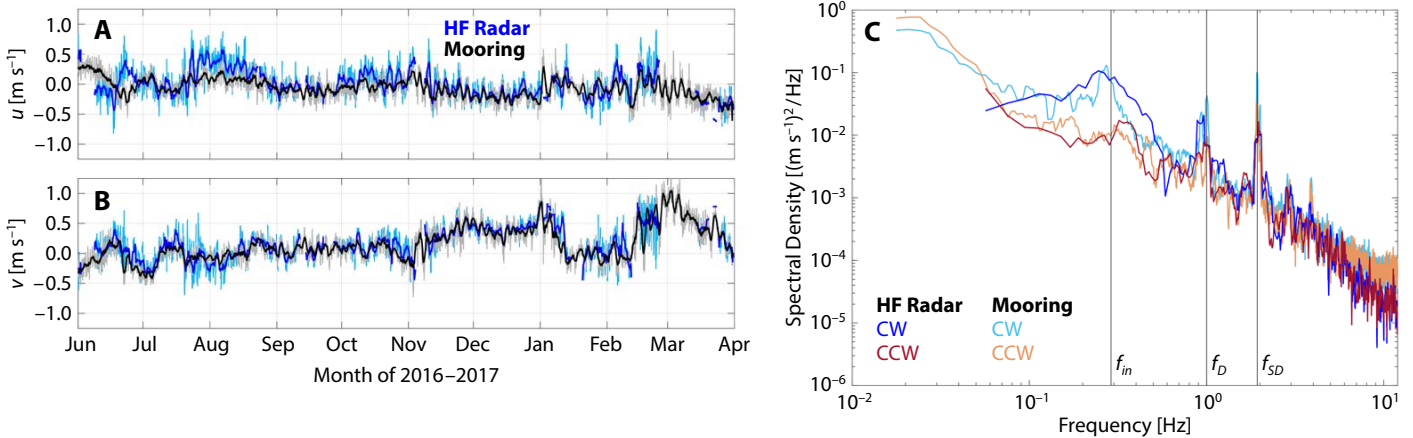


FIGURE 2. (A) Zonal and (B) meridional velocities measured by HF radar (surface, blue) and at the mooring (16–36 m depth, black) show strong agreement northwest of Kayangel (location of mooring shown in Figure 1B). Shaded values are hourly records while the thick lines represent a running 33-hour average to remove tides. (C) Rotary frequency spectra computed from the velocity time series (A, B) capture consistent inertial and tidal peaks.

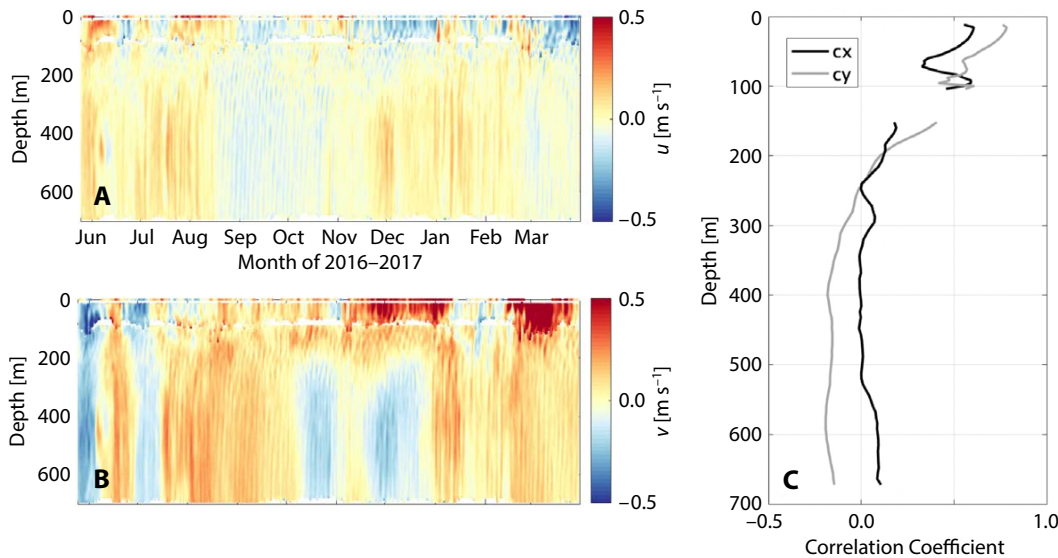


FIGURE 3. Subtidal (A) zonal and (B) meridional currents as a function of depth at the mooring location shown in Figure 1B. Surface values measured by the HF radar are shown at the top of each plot (see Figure 2 for these time series). (C) Correlation coefficients between the surface currents and discrete depths of the moored acoustic Doppler current profiler (ADCP) measurement for zonal (black) and meridional (gray) components. The gap in correlation value represents where no ADCP data are available in the water column.

the west and east generate flow patterns up- and downstream of the island chain, respectively. Composite descriptions of the flow are generated by averaging westward and eastward subtidal velocities in the box shown in **Figure 1B**. During westward incident flow, commonly associated with the NEC, the surface current is topographically blocked and bifurcates approximately 60 km upstream of the island group (**Figure 4A**). Between the deflected flow and the island, a stagnation point forms with observed velocities less than 5 cm s^{-1} . The flow is deflected around both sides of the island where a portion passes over the shallow reefs and through two channels south of Velasco Reef, the 3.5 km wide Kekerel Euchel and 8 km wide Euchelet Ngeruangl channels, located between Kayangel and the main island group. After passing through the channels, the flow recirculates on the western side of the main island (**Figure 4A**). Evidence of flow acceleration, up to three times the mean current, are present in the gaps north and south of the main island group during zonal flows.

Eastward-incident flows that interact

with Palau are generally due to northward migration of the NECC or the transient mesoscale structure of the NEC. For eastward-incident flows, surface currents deflect around Palau, separate, and reattach approximately 60 km downstream (**Figure 4B**). The region in the lee of the island has significantly weaker flows than the flow that reconnects after transiting around Palau.

In addition to the blocked and wake flows associated with westward and eastward incident flows, two additional examples of vorticity generation are used as case studies to diagnose the range of incident flows that interact with the island chain. In early January 2017, a cyclonic eddy with a diameter of 30 km and a Rossby number $Ro \sim 4$ was observed near the coast of Palau, just north of Melekeok (**Figure 5A**). The incident current in this case was from the south, and it followed the coastline to about 7.5°N , where the flow appeared to separate and an eddy formed behind the separation point. The eddy was visible between January 8 and January 13, 2017, after which radar coverage was lost for the subsequent week.

Ro values were persistently larger than 3 within the eddy over the six days of visibility in the radar footprint (**Figure 5B**). These observations suggest that incident flows hitting Palau from oblique angles, in this case from the south, may generate strong vorticity at topography, indicating that the geometry of the island at this incident angle influences the generation.

A second case study occurred on May 21, 2017, when the incident geostrophic flow wrapped around the island chain in a counterclockwise direction (**Figure 5C**). A dipole of counter-rotating eddies was observed that we attribute to the coalescence of (1) an anticyclonic eddy generated by friction and flow separation during eastward flow through the channels between Velasco and the main island, and (2) a mesoscale eddy of positive vorticity likely associated with an NEC meander. The observed vortices had diameters larger than 50 km and $Ro \sim 2$ (**Figure 5D**). Prior to the formation of the anticyclone, the persistent mesoscale cyclone (positive vorticity) was observed for over a week with a diameter over 100 km and $Ro \sim 1$. After the eddies

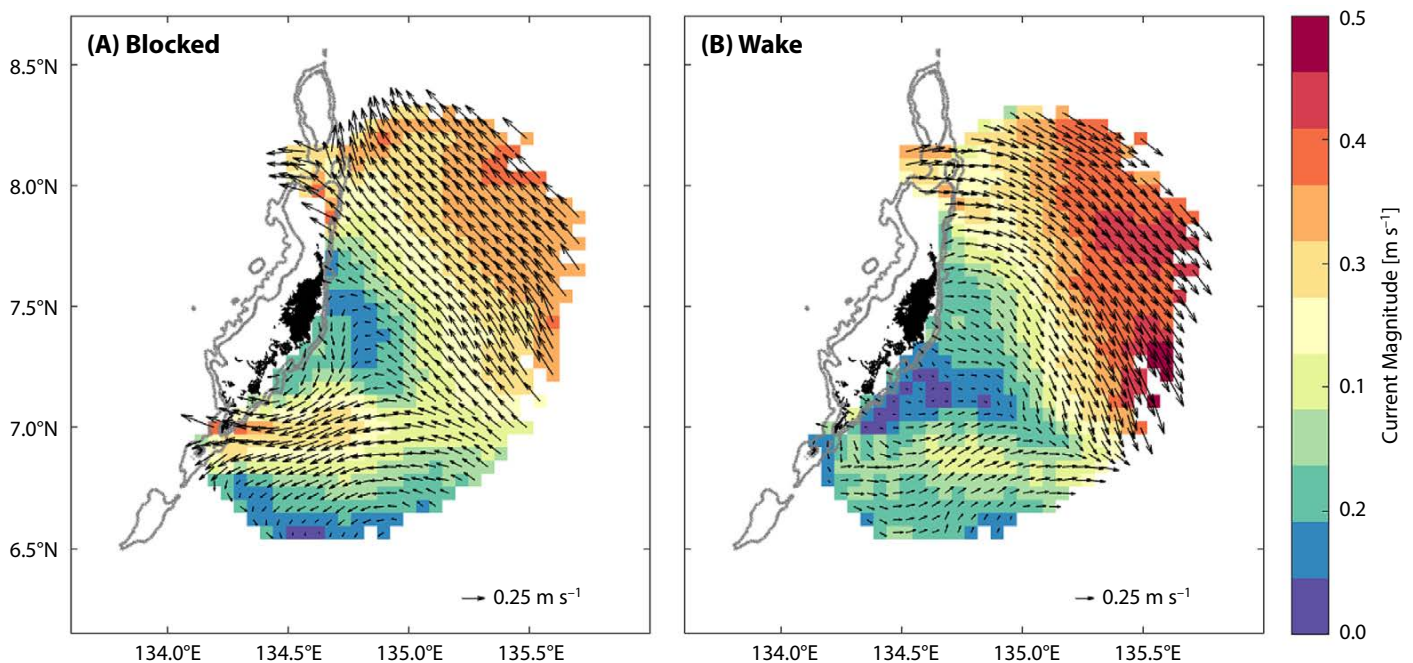


FIGURE 4. Composite images of (A) blocked (incident flow from the east), and (B) wake (incident flow from the west) flow conditions; average current magnitude is shown in colors, and corresponding vectors are indicated by black vectors. During blocked and wake conditions, bifurcation and flow reconnection occur approximately 60 km up- and downstream, respectively.

coalesced, rotational flow speeds in the cyclone increased, its diameter reduced by a half, and Ro doubled. This second case study documents the existence of wake interaction with the mesoscale eddy field, and that vortices consequently shed due to wake instability encounter a persistent mesoscale feature that episodically collides with Palau.

DISCUSSION

This study documents surface current variability in the region surrounding Palau using HF radar measurements. The observations have hourly temporal and

6 km spatial resolution and a range out to 160 km with primary data coverage to the east of the island chain. Data coverage at the three HF sites was limited by a variety of factors, including utility power outages, ionospheric noise, and weak wind conditions, that resulted in a poor scattering environment for derived surface currents. As a result, this paper focuses on case studies and composites of flow variability that capture aspects of blocked flow, wake development, and vorticity production at the island chain of Palau. While our studies are limited by the range and resolution of the radars (160 km and

6 km, respectively), the network's spatial and temporal coverages provide a lens of observation across more than a decade of wavenumbers, and the long dwell time of the observations provides high resolution in the frequency domain. A unique element of our study is the range of water depths across the HF radar footprint. While the majority of coastal studies that use this technology are located in coastal regions dominated by shelf physics (Paduan and Washburn, 2013), our study observes ocean surface currents in a region of steep boundary topography, with average water depths of 4 km. As

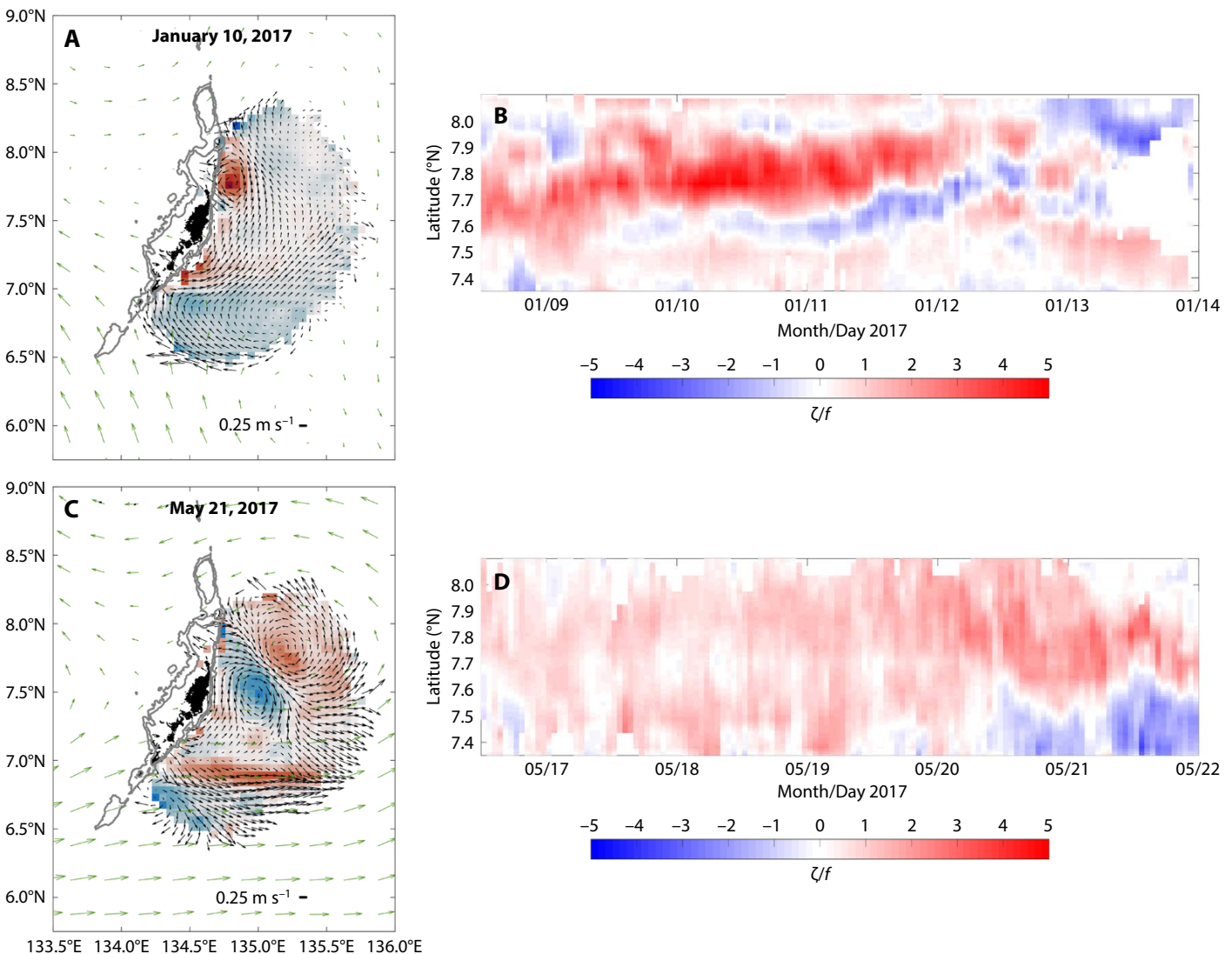


FIGURE 5. Two case studies of vorticity eddies within the HF footprint (A) AVISO geostrophic currents (green vectors), HF radar 33-hour averaged currents (black vectors), and the relative vorticity, ζ , normalized by the planetary vorticity, f , shown in colors. A 30 km diameter eddy forms around 7.5°N and persists for five days along the coast with slight northward translation. (B) Latitudinal Hovmöller diagram of Ro shows the evolution of the vorticity and migration of the eddy along 134.8°E. (C) Same as (A), here depicting an eddy dipole structure. (D) Latitudinal Hovmöller diagram of Ro along 135.15°E shows a mesoscale cyclone that coalesces with an anticyclone on May 20, 2017.

Figure 3 illustrates, the observed surface currents are significantly correlated with subsurface currents that, for our study, extend to thermocline depths of approximately 100 m. This high degree of correlation lends credence to interpretation of the spatial maps beyond the relatively shallow sensing depth of the radar.

The radar-derived surface currents are composed of tidal, inertial, and low-frequency flows. On average, the tidal and inertial currents have speeds of 10–15 cm s⁻¹, with episodic events exceeding 20 cm s⁻¹. The low frequency flow is often dominated by mesoscale variability of the NEC and the NECC. The total incident flow at Palau is broadband in frequency content and changes direction rapidly, adding to the complexity of vorticity generation. Recent studies show that for topography-encountering flows consisting of a mean flow plus an oscillatory (tidal) component, the relative magnitude of each component is important for vorticity generation. MacKinnon et al. (2019) and Johnston et al. (2019, in this issue) observed the formation and shedding of small-scale (~1 km) tidal eddies with varying vertical structure (temperature-salinity interleaving, sheared horizontal velocity, tilting) as incident flows rounded the northern tip

of Velasco Reef and the southern point at Peleliu. Rossby numbers for tidal eddies were ~30, suggesting that ageostrophic flows play a dominant role in vorticity generation at topography. In certain conditions, these eddies were advected downstream and contributed to a broader wake. Zeiden et al. (2019), used velocity profiles from buoyancy gliders to estimate the meridional component of the vorticity 40 km upstream and downstream of the islands. This view of the wake has Ro ~ 0.3, with episodic events of Ro > 1, and the study presents evidence of flow separation and recirculation.

Here, we have used HF radar observations to better understand spatial and temporal variability of the wake at scales intermediate to the studies discussed above. Composite views of blocked and wake flows show zonal incident flow bifurcation and reconnection on the east side of Palau, both of which occur roughly 60 km from the coastline, about one-third of the length of the island chain in the north-south direction. Flows shoreward of the bifurcation are weak, indicating a stagnation point; similar conditions are observed in the downstream lee. Case studies of vortex formation suggest that oblique incident flows, for example, from the south, may separate at sharp

changes in the topography, producing vortices of 30 km scales with Ro ~ 5. A second case study shows the formation of an anticyclonic vortex as flow hits the northern portion of Palau and encounters a mesoscale cyclone. The two vortices, each ~50 km diameter, form a dipole structure with Rossby numbers ~2 that persists for days. Mesoscale features frequently encounter Palau (Andres et al., 2019, in this issue), suggesting that wake interactions with persistent mesoscale features may generate instabilities that contribute to the energy cascade towards smaller scales and turbulence.

Given the complexity of the flows at Palau, a goal of the FLEAT project is to downscale models to incorporate realistic topography and capture submesoscale variability. Here, we use Regional Ocean Modeling System (ROMS) output with one-hour temporal and 800 m spatial resolution, described in Simmons et al. (2019, in this issue), to study details of the wake captured by the HF radar observations. Snapshots of the wake vorticity during eastward flow from the observations (Figure 6A) and the model (Figure 6B) are qualitatively consistent. Flow reconnection on the east side of Palau occurs about 60 km downstream, and vorticity generation at the north and

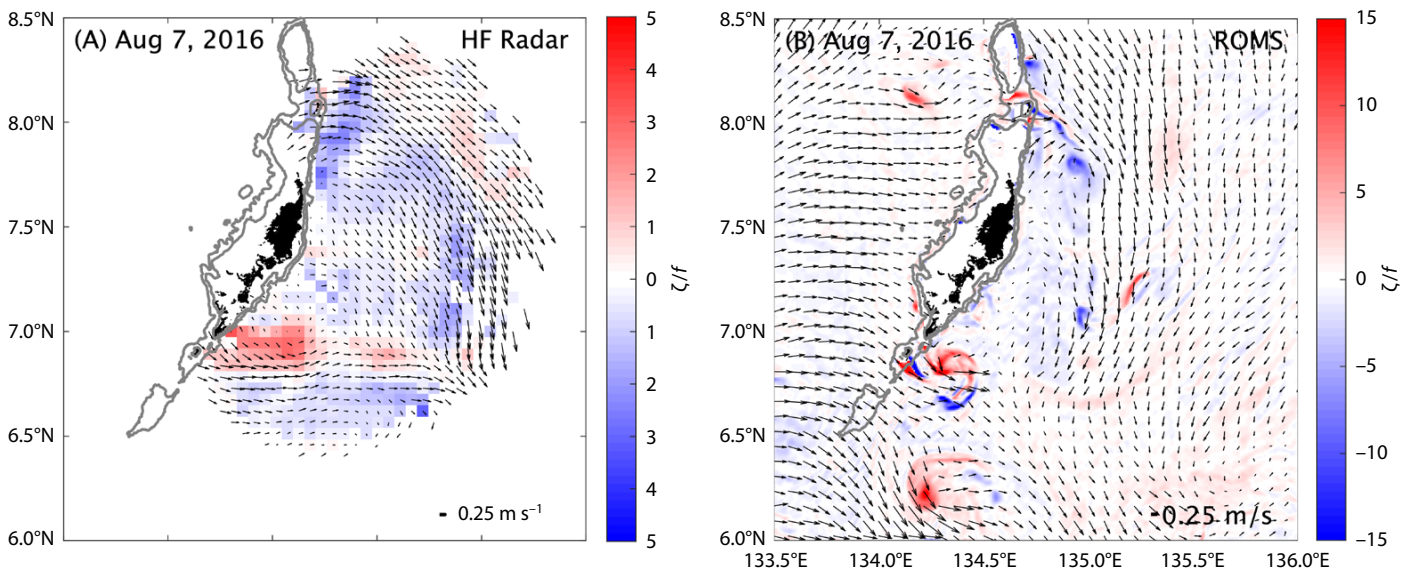


FIGURE 6. Flow patterns during wake conditions from (A) the 6 km resolution HF radar observations, and (B) the 800 m ROMS model output. Relative vorticity normalized by the planetary vorticity (absolute value is the Ro) is shown in background color, and current vectors are shown in black quivers.

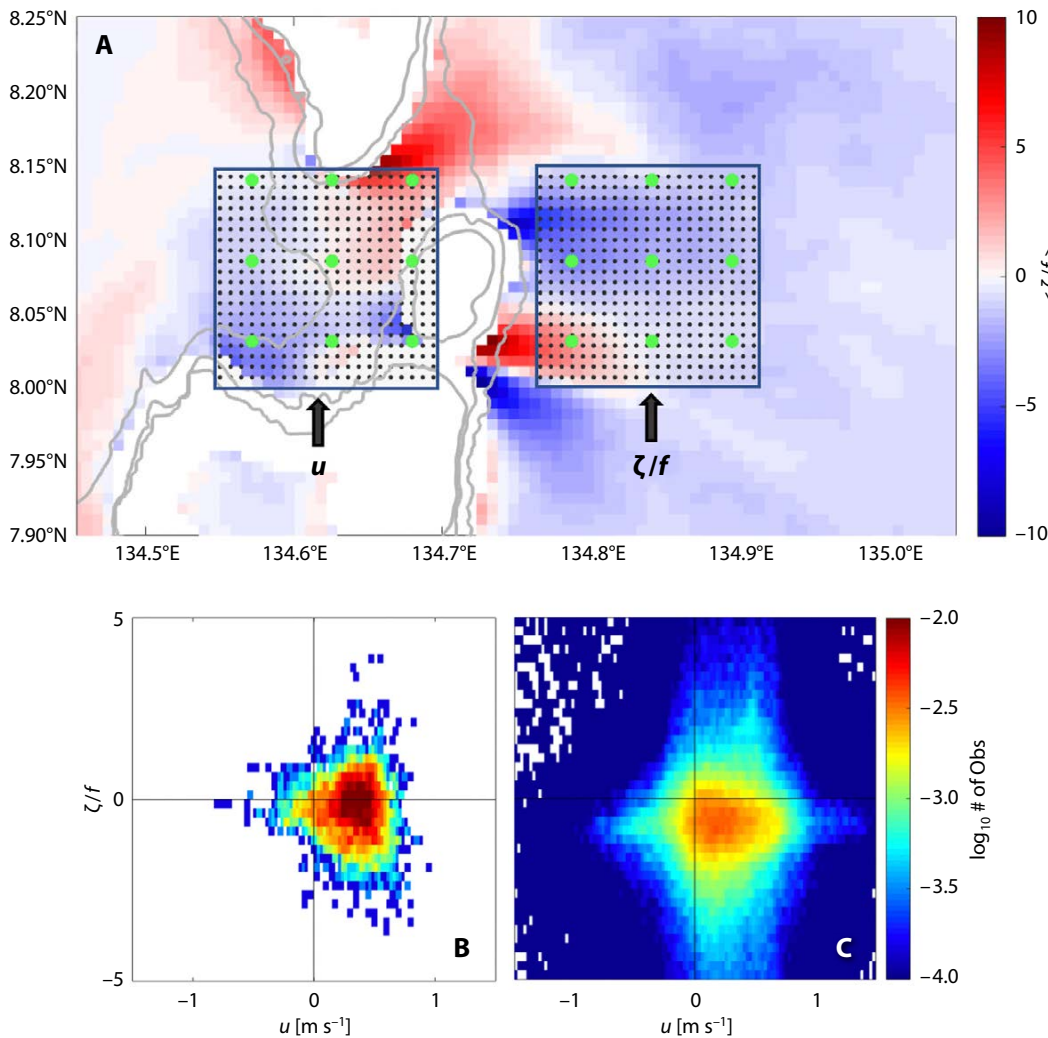


FIGURE 7. (A) One month of observations (July 28–August 28, 2016) at locations marked by green circles, and model output (locations indicated by black circles) are used to study vorticity generation through the channels during predominately eastward flow. The temporally averaged ζ/f is shown in background colors. Probability density functions of upstream (channel, left box) zonal velocity vs. downstream (right box) ζ/f show the nature of vorticity production at the channels in (B) observations and (C) the model.

south points of Palau is negative and positive, respectively. The Rossby numbers in the ROMS model are significantly larger, ~15–20, attributed in part to the spatial resolution (800 m), which is significantly higher than the HF radar currents (6 km).

The high-resolution model highlights the importance of the pass-through channels in the island chain of Palau for vorticity production. The channel widths are comparable to the HF radar spatial resolution; however, the observations capture flow through the channels and vorticity variability on the scale of the channels (Figure 6A). To study vorticity generation during eastward wake conditions, one-month (July 28–August 28, 2016) of model output and observational data are extracted from upstream and downstream boxes (Figure 7A). Probability density functions (Figure 7B,C) of zonal velocity versus ζ/f show that the major-

ity of the vorticity production is negative during eastward flow. Due to the nature of the channels, vorticity of both signs is generated during eastward flow; small-scale vorticity features of both signs are formed in the model, consistent with a coarser perspective from the observations. In addition to the channel geometry, tidal flows can generate vorticity of either sign at times when the oscillatory component exceeds the mean flow. The nearfield wake is composed of vorticity generated by flow through the channels and by flow that rounds the northern side of Velasco Reef. Small-scale features are advected downstream in the model, contributing to enhanced vorticity hundreds of kilometers downstream. While the model doesn't provide phase-resolved details to allow eddy-by-eddy comparisons, statistics of the wake in similar incident flow conditions may provide a

framework for further interpretation of the observations, which will be the subject of future work. The combination of remote sensing, high-resolution modeling, and ongoing data collection provide a unique opportunity for studying wake structure and variability at the remote island nation of Palau, and for characterizing the energetic impact on the large-scale current structure.

SUPPLEMENTARY MATERIALS

The supplementary materials are available online at <https://doi.org/10.5670/oceanog.2019.415>.

REFERENCES

- Andres, M., M. Siegelman, V. Hormann, R.C. Musgrave, S.T. Merrifield, D.L. Rudnick, M.A. Merrifield, M.H. Alford, G. Voet, H.W. Wijesekera, and others. 2019. Eddies, topography, and the abyssal flow by the Kyushu-Palau Ridge near Velasco Reef. *Oceanography* 32(4):46–55, <https://doi.org/10.5670/oceanog.2019.410>.
- Aristegui, J., P. Tett, A. Hernández-Guerra, G. Basterretxea, M.F. Montero, K. Wild, P. Sangrá, S. Hernández-Leon, M. Canton, J.A. García-Braun,

- and others. 1997. The influence of island-generated eddies on chlorophyll distribution: A study of meso-scale variation around Gran Canaria. *Deep Sea Research Part I* 44(7):71–96, [https://doi.org/10.1016/S0967-0637\(96\)00093-3](https://doi.org/10.1016/S0967-0637(96)00093-3).
- Barrick, D.E., M.W. Evans, and B.L. Weber. 1977. Ocean surface currents mapped by radar. *Science* 198(4313):138–144, <https://doi.org/10.1126/science.198.4313.138>.
- Chapman, R.D., L.K. Shay, H.C. Graber, J.B. Edson, A. Karachintsev, C.L. Trump, and D.B. Ross. 1997. On the accuracy of HF radar surface current measurements: Intercomparison with ship-based sensors. *Journal of Geophysical Research* 102(C8):18,737–18,748, <https://doi.org/10.1029/97JC00049>.
- Chung, Y.J., Y.R. Chen, L.Z.H. Chuang, Y.J. Yang, and L.G. Leu. 2017. The correlation analysis of ionospheric clutter and noise using SeaSonde HF radar. In *MTS/IEEE Kobe Techno-Oceans (OTO) 2018 OCEANS*, pp. 1–4, <https://doi.org/10.1109/OCEANSE.2018.8084968>.
- Crombie, D.D. 1955. Doppler spectrum of sea echo at 13.56 Mc/s. *Nature* 175:681–682, <https://doi.org/10.1038/175681a0>.
- Emery, B.M., L. Washburn, and J.A. Harlan. 2004. Evaluating radial current measurements from CODAR high-frequency radars with moored current meters. *Journal of Atmospheric and Oceanic Technology* 21(8):1,259–1,271, [https://doi.org/10.1175/1520-0426\(2004\)021<1259:ERCMF>2.0.CO;2](https://doi.org/10.1175/1520-0426(2004)021<1259:ERCMF>2.0.CO;2).
- Gove, J.M., M.A. McManus, A.B. Neuheimer, J.J. Polovina, J.C. Drazen, C.R. Smith, M.A. Merrifield, A.M. Friedlander, J.S. Eshes, C.W. Young, and A.K. Dillon. 2016. Near-island biological hotspots in barren ocean basins. *Nature Communications* 7:10581, <https://doi.org/10.1038/ncomms10581>.
- Gurgel, K.W. 1994. Shipborne measurement of surface current fields by HF radar. *L'Onde Electrique* 74:54–59.
- Hsin, Y.C., and B. Qiu. 2012. Seasonal fluctuations of the surface North Equatorial Counter-current (NECC) across the Pacific Basin. *Journal of Geophysical Research* 117(C06), <https://doi.org/10.1029/2011JC007794>.
- Hsu, P.C., K.H. Cheng, S. Jan, H.J. Lee, and C.R. Ho. 2019. Vertical structure and surface patterns of Green Island wakes induced by the Kuroshio. *Deep Sea Research Part I* 143:1–16, <https://doi.org/10.1016/j.dsr.2018.11.002>.
- Johnston, T.M.S., J.A. MacKinnon, P.L. Colin, P.J. Haley Jr., P.F.J. Lermusiaux, A.J. Lucas, M.A. Merrifield, S.T. Merrifield, C. Mirabito, J.D. Nash, and others. 2019. Energy and momentum lost to wake eddies and lee waves generated by the North Equatorial Current and tidal flows at Peleliu, Palau. *Oceanography* 32(4):110–125, <https://doi.org/10.5670/oceanog.2019.417>.
- Kundu, P.K., and I. Cohen. 2002. *Fluid Mechanics*, Academic Press, New York.
- Lipa, B., and D. Barrick. 1983. Least-squares methods for the extraction of surface currents from CODAR crossed-loop data: Application at ARSLOE. *IEEE Journal of Oceanic Engineering* 8(4):226–253, <https://doi.org/10.1109/JOE.1983.1145578>.
- MacKinnon, J.A., M.H. Alford, G. Voet, K. Zeiden, T.S. Johnston, M. Siegelman, S. Merrifield, and M. Merrifield. 2019. Eddy wake generation from broadband currents near Palau. *Journal of Geophysical Research* 124(7):4,891–4,903, <https://doi.org/10.1029/2019JC014945>.
- Ohlmann, C., P. White, L. Washburn, E. Terrill, B. Emery, and M. Otero. 2006. Interpretation of coastal HF radar-derived surface currents with high-resolution drifter data. *Journal of Atmospheric and Oceanic Technology* 24:666–680, <https://doi.org/10.1175/JTECH1998.1>.
- Paduan, J.D., and L. Washburn. 2013. High-frequency radar observations of ocean surface currents. *Annual Review of Marine Science* 5:115–136, <https://doi.org/10.1146/annurev-marine-121211-172315>.
- Pattiaratchi, C., A. James, and M. Collins. 1987. Island wakes and headland eddies: A comparison between remotely sensed data and laboratory experiments. *Journal of Geophysical Research* 92(C1):783–794, <https://doi.org/10.1029/JC092iC01p00783>.
- Qiu, B., and R. Lukas. 1996. Seasonal and inter-annual variability of the North Equatorial Current, the Mindanao Current, and the Kuroshio along the Pacific western boundary. *Journal of Geophysical Research* 101:12,315–12,330, <https://doi.org/10.1029/95JC03204>.
- Schmidt, R. 1986. Multiple emitter location and signal parameter estimation. *IEEE Transactions on Antennas and Propagation* 34(3):276–280, <https://doi.org/10.1109/TAP.1986.1143830>.
- Schramek, T.A. 2018. *Ocean-Island Interactions in the Western Pacific*. Doctoral dissertation, UC San Diego, 133 pp.
- Schönau, M.C., and D.L. Rudnick. 2015. Glider observations of the North Equatorial Current in the western tropical Pacific. *Journal of Geophysical Research* 120(5):3,586–3,605, <https://doi.org/10.1002/2014JC010595>.
- Siegelman, M., M.A. Merrifield, E. Firing, J.A. MacKinnon, M.H. Alford, G. Voet, H.W. Wijesekera, T.A. Schramek, K.L. Zeiden, and E.J. Terrill. 2019. Observations of near-inertial surface currents at Palau. *Oceanography* 32(4):74–83, <https://doi.org/10.5670/oceanog.2019.413>.
- Simmons, H.L., B.S. Powell, S.T. Merrifield, S.E. Zedler, and P.L. Colin. 2019. Dynamical down-scaling of equatorial flow response to Palau. *Oceanography* 32(4):84–91, <https://doi.org/10.5670/oceanog.2019.414>.
- Stewart, R.H., and J.W. Joy. 1974. HF radio measurements of surface currents. *Deep Sea Research and Oceanographic Abstracts* 21(12):1,039–1,049, [https://doi.org/10.1016/0011-7471\(74\)90066-7](https://doi.org/10.1016/0011-7471(74)90066-7).
- Smith, W.H.F., and D.T. Sandwell. 1997. Global sea floor topography from satellite altimetry and ship depth soundings. *Science* 277:1,957–1,962, <https://doi.org/10.1126/science.277.5334.1956>.
- Sugimoto, T., S. Kimura, and K. Tadokoro. 2001. Impact of El Niño events and climate regime shift on living resources in the western North Pacific. *Progress in Oceanography* 49(1–4):113–127, [https://doi.org/10.1016/S0079-6611\(01\)00018-0](https://doi.org/10.1016/S0079-6611(01)00018-0).
- Weller, R.A. 1982. The relation of near-inertial motions observed in the mixed layer during the JASIN (1978) experiment to the local wind stress and to the quasi-geostrophic flow field. *Journal of Physical Oceanography* 12(10):1,122–1,136, [https://doi.org/10.1175/1520-0485\(1982\)012<1122:TRONIM>2.0.CO;2](https://doi.org/10.1175/1520-0485(1982)012<1122:TRONIM>2.0.CO;2).
- Zeiden, K.L., D.L. Rudnick, and J.A. MacKinnon. 2019. Glider observations of a meso-scale oceanic island wake. *Journal of Physical Oceanography* 49(9):2,217–2,235, <https://doi.org/10.1175/JPO-D-18-0233.1>.
- Zhang, Z., H. Xue, F. Chai, and Y. Chao. 2017. Variability of the Pacific North Equatorial Current from 1993 to 2012 based on a 1/8° Pacific model simulation. *Journal of Geophysical Research: Oceans* 122(3):2,382–2,400, <https://doi.org/10.1002/2016JC012143>.

ACKNOWLEDGMENTS

Logistical and field support were provided by members of the Coral Reef Research Foundation (CRRF) and the Coastal Observing Research and Development Center (CORDC): Lori Colin, Sharon Patris, Gerda Ucharm, Andy Nager, Mike Jilka, Myles Syverud, Sean Celona, John Swords, and Eric Gallimore. The authors wish to acknowledge the people and government of Palau for welcoming marine science in their country, with special acknowledgment to the Bureau of Marine Resources and the various state offices that provided research permits to conduct this study. The OSCAR data were obtained from JPL Physical Oceanography DAAC and developed by ESR. AVISO data shown are total geostrophic currents obtained from delayed time (DT) merged all satellites Global Ocean Gridded SSALTO/DUACS Sea Surface Height L4 product at <http://marine.copernicus.eu>. This work was funded by the US Office of Naval Research under grant N00014-15-1-2304 as part of the Flow Encountering Abrupt Topography (FLEAT) Departmental Research Initiative and was made possible by the vision of and support from Theresa Paluszkiwicz and Scott Harper.

AUTHORS

Sophia T. Merrifield (smerrifield@ucsd.edu) is Project Scientist, Scripps Institution of Oceanography, University of California San Diego (SIO-UCSD), La Jolla, CA, USA. **Patrick L. Colin** is Director, Coral Reef Research Foundation, Koror, Palau. **Thomas Cook** is Systems Integration Engineer, **Carlos Garcia-Moreno** is Systems Integration Engineer, **Jennifer A. MacKinnon** is Professor, **Mark Otero** is Programmer/Analyst, and **Travis A. Schramek** is an oceanographer, all at SIO-UCSD, La Jolla, CA, USA. **Mika Siegelman** is a PhD Candidate, School of Ocean and Earth Science and Technology, University of Hawai'i at Mānoa, Honolulu, HI, USA. **Harper L. Simmons** is Associate Professor, College of Fisheries and Ocean Sciences, University of Alaska Fairbanks, Fairbanks, AK, USA. **Eric J. Terrill** is Director, Coastal Observing Research and Development Center, SIO-UCSD, La Jolla, CA, USA.

ARTICLE CITATION

Merrifield, S.T., P.L. Colin, T. Cook, C. Garcia-Moreno, J.A. MacKinnon, M. Otero, T.A. Schramek, M. Siegelman, H.L. Simmons, and E.J. Terrill. 2019. Island wakes observed from high-frequency current mapping radar. *Oceanography* 32(4):92–101, <https://doi.org/10.5670/oceanog.2019.415>.

COPYRIGHT & USAGE

This is an open access article made available under the terms of the Creative Commons Attribution 4.0 International License (<https://creativecommons.org/licenses/by/4.0/>), which permits use, sharing, adaptation, distribution, and reproduction in any medium or format as long as users cite the materials appropriately, provide a link to the Creative Commons license, and indicate the changes that were made to the original content.